Study of UV aging on the performance characteristics of vegetable oil and palm oil derived isocyanate based polyurethane

Sonalee Das[†], Priyanka Pandey, Smita Mohanty, and Sanjay Kumar Nayak

Laboratory for Advanced Research in Polymeric Materials, Central Institute of Plastics Engineering and Technology,
Bhubaneswar, Odisha-751024, India

Abstract–The impact of UV aging on the characteristic properties of synthesized polyurethane (PUs) from castor oil and transesterified castor oil with palm oil based isocyanate and 1,4 butanediol was investigated at different exposure time of 0, 250, 500, 750 and 1,000 h, respectively. The aging properties of the PU films were analyzed through differential scanning calorimetry (DSC), Fourier transform infrared spectroscopy (FTIR), X-ray photoelectron spectroscopy (XPS), Scanning electron microscopy (SEM) and Tensile tests. The PU films derived from castor oil showed noticeable changes in chemical structure after 250 h of UV exposure owing to chain scission of the urethane group. A considerable decrease in the thermal and tensile properties of the developed PU films was observed due to the plasticization phenomenon. SEM micrographs revealed morphological changes through the appearance of cracks and blisters composed of primary amines on the surface of exposed PU films. However, PUs derived from transesterified castor oil with a higher hydroxyl value exhibited improved UV resistance characteristics due to higher crosslinking and degrade only after 750 h of exposure. Thus, the synthesized green PUs based on transesterified castor oil with palm oil based isocyanate compositions can be candidate materials for developing UV resistant coating material.

Keywords: Transesterified Castor Oil, UV Aging, Chain Scission, Blisters, Palm Oil Based Isocyanate

INTRODUCTION

Polyurethane (PUs) resins have gained enormous interest in the field of coatings [1-3] owing to excellent chemical as well as abrasion resistance, toughness, high tensile and tear strength [4]. However, these coatings are generally exposed to harsh environmental conditions that include UV, thermal and hydrothermal exposure, which leads to degradation and reduces the long-term applicability of these materials. Hence, in order to achieve reliable coating for a long term application the coating formulations of polyurethane should be extremely resistant to the weathering conditions [5,6]. In spite of being in consideration for past few years, the long-term properties of polyurethane, specifically derived from biobased components in terms of UV resistance have not been adequately addressed and are still in detailed investigation. The influence of UV aging has attracted huge interest with respect to other environmental conditions since it provides molecular level information about degradation process as well as determines the service conditions of tested material within less span of time [7,8-10]. Thus, extensive information concerning the degradation behavior of polyurethane over a prolonged period of time needs to be evaluated to predict its lifetime reliability [11].

Moreover, the increasing demand of renewable resource based materials along with reduced volatile organic content (VOCs) emission renders the utilization of plant based polyol and isocyanate

for polyurethane synthesis [12]. In this context, this study considers the utilization of castor oil based polyol and palm oil based isocyanate for polyurethane synthesis. Furthermore, since the hydroxyl functionality of the polyol component plays a vital role towards deciding the performance of polyurethane [13-16] an attempt to modify the hydroxyl functionality of castor oil via. transesterification was also undertaken and the effect of various amounts of transesterification reagent (i.e., pentaerythritol) was analyzed.

Based on our preliminary study, the polyurethane synthesis was performed at the optimized NCO : OH molar ratio of 1.4 : 1 [17]. The optimum composition of transesterification reagent was obtained from the physicochemical analysis. Further, a comparative aspect of the optimum composition of polyurethane prepared with castor oil and transesterified castor oil was also established in terms of UV resistant characteristics analyzed on the basis of chemical, physical, morphological and mechanical changes.

The study reveals that the polyurethane prepared using transesterified castor oil exhibits better UV resistant characteristics as compared to unmodified castor oil based polyurethanes.

EXPERIMENTAL

1. Materials and Methods

Partially aliphatic palm oil based polymeric isocyanate (PoIs) was provided by M/s. Vencorex Chemical, France. Castor oil (CO) was purchased from M/s.SD Fine chemicals (Kolkata, India). Pentaerythritol (PE), Lead oxide catalyst (PbO) and 1, 4 butanediol chain extender (1, 4 BD) were procured from M/s Himedia, India. The catalyst dibutyltin dilaurate (DBTDL) was purchased from M/s.

Table 1. Details regarding the acid value, hydroxyl number and viscosity of polyols

Sample code	PE/CO molar ratio	Acid value[a] (mg KOH/g)	Viscosity[b] (cps) at 25 °C	M_w[c] (g/mol)	Unsaturated double bond
CO	0	1.96	890	933	3
MCO 0.1	0.1 : 1	1.68	980	3490	1
MCO 0.2	0.2 : 1	1.40	992	3931	1
MCO 0.3	0.3 : 1	1.21	1020	4081	1

Note: Acid value[a] was determined as per ASTM D 1824, viscosity[b] determined as per ASTM D 7253 and M_w[c] was determined using gel permeation chromatography (GPC) technique

Sigma Aldrich, Germany.

2. Transesterification of Castor Oil (CO)

The transesterification of castor oil using pentaerythritol was well described in our earlier literature report [17]. The transesterification of castor oil was performed at three different pentaerythritol (PE) : castor oil (CO) molar ratios, 0.1 : 1, 0.2 : 1 and 0.3 : 1, in presence of PbO catalyst; and the resulting polyols were designated as MCO 0.1, MCO 0.2 and MCO 0.3, respectively. The hydroxyl value of CO, MCO 0.1, MCO 0.2 and MCO 0.3 was found to be 160, 190, 234 and 270 mgKOH/g, respectively, as per ASTM 1957. The acid value, molecular weight and viscosity of CO, MCO 0.1, MCO 0.2 and MCO 0.3 [17] are summarized in Table 1.

3. Synthesis of Chain Extended Polyurethane (PUs)

PUs were synthesized at a constant NCO/OH molar ratio of 1.4 : 1, using a well established method as documented in our earlier literature report [18]. Two types of polyurethane were synthesized using raw castor oil and transesterified castor oil as polyol component with PoIs. PUs synthesized using castor oil, PoIs and chain extender (1, 4 BD) was referred to as UBPU and that of synthesized from transesterified castor oil, MCO 0.1, MCO 0.2 and MCO 0.3, PoIs and 1, 4 BD were referred to as MBPU 0.1, MBPU 0.2 and MBPU 0.3, respectively. The reactions were carried out in an inert nitrogen atmosphere at 60-75 °C for 1-1.5 h. The films cast onto Teflon sheets and coated polycarbonate substrate were allowed to cure at 90 °C for 12 h. Details of composition of synthesized PUs are given in Table 2.

4. UV Aging

UV aging test was performed using M/s. Q-Lab Corporation, QUV Accelerated Weathering Equipment following the ASTM Standard G 53-96. The film samples of dimension (10×10) cm were alternately exposed to UV radiation of 8 h at 60 °C followed by

Table 2. Information regarding the composition and weight of the reactants for PU synthesis

Sample code	CO (ml)	MCO (ml)	PoIs (ml)	1,4 BD (ml)	Hard segment* (wt%)
UBPU	30	0	38.3	10	61.6
MBPU 0.1	0	30	40.1	10	62.5
MBPU 0.2	0	30	43.8	10	64.2
MBPU 0.3	0	30	46.1	10	65.1

Note: Hard segment (wt%) $^* = \dfrac{\text{Wt of (1,4BD + PoIs)}}{\text{Wt of (1,4BD + PoIs)} + \text{Wt of (CO/MCO)}}$

water condensation of 8 h at 50 °C in a cyclic manner. The samples were subjected to UV exposure for 250 h, 500 h, 750 h and 1,000 h of durations.

CHARACTERIZATION

1. Fourier Transform Infrared Spectroscopy (FTIR)

The FTIR spectra were recorded and analyzed within the range of 4,000-400 cm^{-1} using M/s. Nicolet 6700, Thermo Scientific, USA with omnic software for data collection and to study the chemical changes under UV exposure. The FTIR study was carried out at regular interval of (a) 0 h (b) 250 h (c) 500 h (d) 750 h and (e) 1,000 h duration to investigate the effect of weathering on the structural modification. For a precise comparison of the characteristic FTIR peaks, all spectra were normalized using the -CH band at 2,927 cm^{-1}.

2. Solid State Nuclear Magnetic Resonance Spectroscopy (NMR)

^{13}C NMR studies of the unexposed and exposed PU samples were carried out using M/s. Jeol Resonance 400 MHZ spectrometer to investigate the nature and effect of UV degradation.

3. X-Ray Photoelectron Spectroscopy (XPS)

XPS surface analysis was performed with ESCA omicron nanotechnology oxford instruments to analyze the elemental composition using MgKα radiation (λ=1,486.7 eV) operated under 5×10^{-9} torr. XPS spectra were acquired at 45° with pass energy of 178.9 eV for survey scans.

4. Gel Permeation Chromatography (GPC)

Molecular weight (Mw) and polydispersity index (PDI) of the respective MCOs and CO polyol were studied by Waters instrument, consisting of a 515 pump and a 410 differential refractometer. The THF flow rate was maintained at 0.6 mL/min. Samples diluted in THF (10 mg/10 ml) were filtered through a 0.45 μm molecular sieve.

5. Photo-oxidation Index (PI) and Carbonyl Index (CI)

For further quantitative comparison regarding the degree of aging, the PI and CI were calculated from the FTIR spectra. Photo-oxidation is the phenomenon of degradation of polymers in the presence of oxygen/ozone, and carbonyl index assesses the polymer degradation degree by quantification of absorption bands assigned to carbonyl groups. These two parameters were determined by using Eqs. (1) and (2), respectively [19]:

$$PI = (A/B)_{aged} - (A/B)_{initial} \qquad (1)$$

$$CI = C/B \qquad (2)$$

wherein, A corresponds to υ (-NH) peak area corresponding to 3,720-3,050 cm^{-1} while, B and C represent the υ (-CH$_3$) and υ (-C=O) peak area corresponding to 2,926-2,860 cm^{-1} and 1,780-1,665 cm^{-1}, respectively. For a precise quantitative comparison regarding the degree of aging, the (-CH) peak was taken as the internal standard. The area beneath the abovementioned peaks was determined using M/s. Nicolet 6700, Thermo Scientific, USA, omnic (3.0) software program.

6. Scanning Electron Microscopy (SEM)

For investigating the influence of UV exposure on the morphological features of polyurethane, SEM micrographs of the samples fractured under cryo conditions were analyzed using EVO MA 15, M/s. Carl Zeiss, Germany, was employed to obtain the SEM images.

7. Tensile Properties

Tensile tests were performed using UTM (M/s Instron Instruments Ltd., UK) at 25 °C as per ASTM D882-91 to analyze the impact of UV exposure on the tensile properties of PUs. The cross-head speed used was 10 mm/min. The presented result was an average of five tests for each sample.

8. Differential Scanning Calorimetry (DSC Analysis)

Thermal stability of PUs was measured using DSC analysis at a heating rate of 10 °C/min under nitrogen flow from −70 to 100 °C to determine the effect of UV aging on the glass transition temperature (T$_g$).

9. Cross-linked Fraction

The cross linking fraction (CLF) of the polyurethane samples was used to assess the impact of UV exposure on the cross linking degree through sol gel analysis. Rectangular PU film sample with dimension 12 mm×15 mm×1 mm (length×width×thickness) of known weight was dipped in 30 ml of chloroform solution for 24 h at ambient temperature. Thereafter, the swollen films were removed and dried in a vacuum oven and weighed to determine M$_{sf}$ (mass of swollen film). The residual solution from the swollen films was then evaporated and the remaining polymer residue was again dried in a vacuum oven to determine M$_s$ (mass of sol fraction). Then the cross-linked fraction was determined by using Eq. (3),

$$CLF, \text{wt}\% = \frac{M_{sf} + M_s}{M_{sf}} \times 100 \tag{3}$$

10. Yellowness Index (ΔYI) and Color Difference (ΔE*)

The weathering durability test of the exposed PU films was determined by calculating the yellowness index (ΔYI) and analyzing the color difference. The ΔYI was investigated as per ASTM E313-98 by placing the free films on black background. The yellowness index of both the films was determined before (0 h) and after (1,000 h) of UV exposure, respectively, and thereafter subtracted to determine ΔYI:

$$\Delta YI = YI_A - YI_B \tag{4}$$

where YI$_A$ is the yellowness index after UV exposure and
    YI$_B$ is the yellowness index before UV exposure.

The change in color prior and after UV aging was measured by spectrophotometer (Gretag Macbeth, Color eye-7000A, USA) as per the standard CIE 1976. The color parameter values, ΔL*, Δa* and Δb*, were calculated to determine the surface color difference (ΔE*) to evaluate the photochemical degradation. The ΔL* depicts the grey value and ranges from 100 (white) to 0 (black) and higher ΔL* indicates higher greyness and vice versa, while both Δa* and Δb* are the chromaticity coordinates. The Δa* value indicates the redness/greenness and +Δa* value=redness and −Δa* value=greenness. On the other hand, Δb* signifies yellowness/blueness and +Δb* value=yellowness and −Δb* value=blueness. The ΔE* value was calculated by using the formula [9]

$$\Delta E^* = \left[\sqrt{\Delta L^{*2} + \Delta a^{*2} + \Delta b^{*2}} \right] \tag{5}$$

where, $\Delta L^* = L_f^* - L_i^*$,
    $\Delta a^* = a_f^* - a_i^*$,
    $\Delta b^* = b_f^* - b_i^*$,

i and f denotes the initial and final values.

11. Nanoindentation

Nanoindentation measurement characterizes the surface mechanical and viscoelastic properties of the material to investigate the impact of UV degradation. Nanoindentation was carried out by using a UMIS Nanoindentation system (M/s. Frisher-Cripps, Australia) with a Berkovich indenter of tip radius 150 nm and face angle of 63.5°. The test was performed using a load of 5 mN, and for each specimen at least ten indentations were carried out at different positions of the film, and the average value was reported. The maximum load was kept for 30 s in the recovery stage for minimizing the viscoelastic effect of the polymer during the stage of unloading (creep time).

The composite modulus 'E$_r$' required for calculating the elastic modulus 'E' was determined by utilizing the contact stiffness 'S' derived from regression function at the beginning of unloading and contact area 'A' as signified in Eq. (6). The value of 'A' is obtained from Eq. (7) by using the calibration function 'f' [20],

$$E_r = \frac{\sqrt{\pi}}{2\beta} \frac{S}{\sqrt{A}} \tag{6}$$

$$A = 24.5 h_c^2 \tag{7}$$

where β is the correction factor for the indenter shape (β=1.07).
    E is determined by using Eq. (8),

$$\frac{1}{E_r} = \frac{1 - \upsilon^2}{E} + \frac{1 - \upsilon_i^2}{E_i} \tag{8}$$

where E$_i$ is the total elastic compliance and υ is Poisson's ratio.

Hardness (H) is the resistance against plastic deformation and which can be determined by using Eq. (9),

$$H = \frac{F_{max}}{A} \tag{9}$$

12. Wettability Studies (Contact Angle)

The contact angle and surface free energy were determined to investigate the effect of UV irradiation on the wettability of the exposed samples. The contact angle was measured at room temperature using M/s Phoenix SEO instrument with three different probe test liquids: water, diiodomethane and methanol. For each specimen five readings were collected and the average value was reported. These three probe liquids with different surface tension

values (γ_l) were also utilized to determine the surface free energy by means of Wu and Nancollas [21] and Owens and Wendt model [22], following Eqs. (10), (11) and (12).

$$\gamma_{lv}(1+\cos\Theta)=4\left(\frac{\gamma_{sv}^p\gamma_{lv}^p}{\gamma_{sv}^p+\gamma_{lv}^p}+\frac{\gamma_{sv}^d\gamma_{lv}^d}{\gamma_{sv}^d+\gamma_{lv}^d}\right) \tag{10}$$

$$\gamma_{lv}(1+\cos\Theta)=2\sqrt{\gamma_{sv}^p\gamma_{lv}^p}+2\sqrt{\gamma_{sv}^d\gamma_{lv}^d} \tag{11}$$

$$\gamma_{sv}=\gamma_{sv}^p+\gamma_{sv}^d \tag{12}$$

where, γ_{lv} is the liquid vapour interfacial tension,
Θ is Young's contact angle,
γ_{sv}^p and γ_{sv}^d are the polar and dispersive factor of the surface free energy of the solid,
γ_{lv}^p and γ_{lv}^d are the polar and dispersive factor of the surface tension of the probe liquid and,
γ_{sv} is the total surface free energy of solid.

The γ_{lv} of water, diiodomethane and benzyl alcohol is 72.8, 50.8 and 40 mN/m. The and of water, diiodomethane and benzyl alcohol are 51, 0.4, 11.4 mN/m and 21.8, 50.8 and 28.6 mN/m respectively.

13. Matrix Assisted Laser Desorption (MALDI-TOF Analysis)

MALDI TOF MS method was used to confirm the successful synthesis of MCO. It was done by a comparative analysis between the components of alcoholysis product present in CO and MCO respectively. MALDI TOF measurement of raw CO and MCO was done with M/s. Shimadzu biotech AXIMA performance MALDI/TOF model. Linear mode was used to detect positive ions, and the accelerated voltage used was 20 kV. To produce laser desorption nitrogen laser operating at 107 Hz was used. Dithranol was used as the matrix and samples were dissolved in the methanol/water mixture with a concentration of 1 g/ml. The matrix solution and the sample solution were mixed in 1:1 ratio and from this solution 0.5-1 µl was deposited onto stainless steel plate and allowed to air dry prior to taking the spectra.

14. Properties of the Developed Polyurethane Coating

The optimum composition of transesterification reagent (i.e., pentaerythritol) was obtained by investigating the physical properties of the polyurethane coatings. The abrasion resistance of the PC coated films was determined as per ASTM D 4060, using (M/s. Taber Model 530 Abraser) in terms of weight loss per 1000 cycles using CS 10 wheel with a load of 500 g each [18]. The pot life, viscosity and drying time of the respective polyurethane coatings

were measured as per BIS method [27]. The mechanical properties of the PU coating were also characterized for determining the scratch hardness, impact and abrasion resistance, respectively. The impact strength of polyurethane coatings was measured as per ASTM D 2794-93 based on the striking height on the coated panels without cracking. The scratch hardness of coated samples was determined by using (M/s. Sheen scratch hardness tester) as per BS3900.

RESULTS AND DISCUSSION

1. Physical Properties of the Coating Formulation

It is observed from Table 3 that polyurethane derived from transesterified castor oil exhibits faster drying time as compared to polyurethane derived from neat castor oil owing to the high hydroxyl value of polyol, which provides cross-linking site for the formation of cross-linked polymer network promoting faster curing reaction [13]. In case of transesterified polyurethane, as the hydroxyl value increases the drying time also decreases; however, MBPU 0.3 takes longer duration for drying as compared with MBPU 0.2 and MBPU 0.1. This might be due to the increase in the hydroxyl group per mg of sample and higher molecular weight of the polyol MCO 0.3, which decreases the % NCO content in the polyurethane, lowering the availability of reactive sites and thereby delaying the curing reaction in MBPU 0.3 [16].

The results in Table 3 show that the viscosity of transesterified polyurethane increases with a substantial increase in the amount of PE, which might be due to the increased hydroxyl value of polyol. Higher viscosity of MBPU 0.3 as compared to UPBPU, MBPU 0.1 and MBPU 0.2 leads to the requirement of higher amount of solvent to obtain desirable viscosity of MBPU 0.3 in order to prepare the uniform flawless coating. The use of such high amount of solvent not only represents an economic disadvantage, but also increases the VOC emission to the atmosphere since the solvent is lost by evaporation and does not form a part of the final coating [24]. Moreover, MBPU 0.3 exhibits shorter pot life as compared with other compositions due to higher viscosity and higher number of functional groups [25].

The mechanical properties of polyurethane coatings indicate that the transesterification of castor oil leads to higher scratch hardness, abrasion resistance and impact strength as compared to the unmodified castor oil counterpart. This is due to the increase in the amount of OH content in transesterified castor oil that leads

Table 3. Physical and mechanical properties of synthesized PU

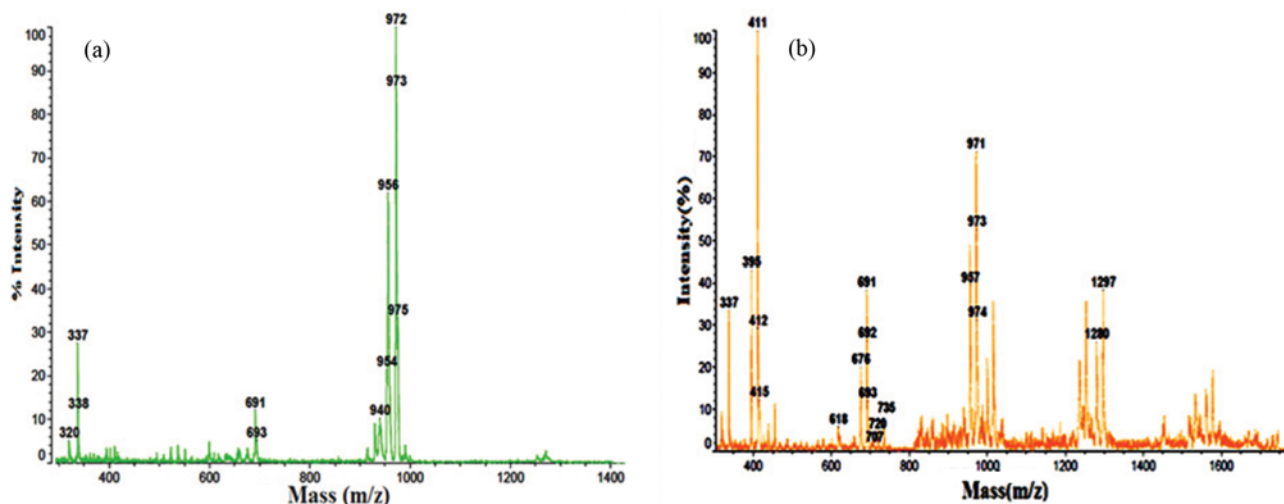| Characteristic	UBPU	MBPU 0.1	MBPU 0.2	MBPU 0.3
Viscosity (cps) 25 °C	2120	3564	3895	4325
Drying time (mins)				
• Surface dry	240±0.2	190±0.5	150±0.3	170±0.7
• Tack free dry	600±0.7	170±0.2	120±0.4	160±0.3
Pot life (mins)	300±0.1	250±0.6	220±0.4	170±0.2
Abrasion resistance (mg/1000 cycles)	7.4±0.1	4.6±0.3	2.7±0.7	3.5±0.2
Impact resistance (J)	10.3±0.4	5.06±0.3	3.23±0.3	4.56±0.1
Scratch hardness (kg)	2±0.1	3.5±0.6	4.7±0.1	5.1±0.3

Fig. 1. Mass spectra of (a) CO and (b) MCO 0.2 for the range of 200-1400 m/z.

to increased hydroxyl value and hence higher degree of crosslinking [13,18]. Moreover, it is observed that with an increase in PE content the rigidity of the system increased in the following order: MBPU 0.3>MBPU 0.2>MBPU 0.1. This increase in rigidity of the system results in lowering of abrasion resistance and impact strength in MBPU 0.3 due to brittle failure [16].

Thus, the results indicate that transesterified castor oil based polyurethane exhibits higher mechanical and faster drying properties as compared with unmodified castor oil based polyurethanes. Therefore, based on the above observations, MBPU 0.2 (synthesized using MCO 0.2 and PoIs) was chosen as the optimized composition with balanced viscosity and coating characteristics amongst the MBPUs and considered for further investigation.

2. Matrix Assisted Laser Desorption (MALDI-TOF Analysis)

MALDI TOF spectrum of CO in the range of 200-1400 m/z is represented in Fig. 1(a). The intense peak observed at 972 m/z corresponds to to the potassiated ions of the triricinolein, the peak at m/z 956 corresponds to the sodiated ions of the triricinolein, the most abundant castor oil triglyceride [26]. This triricinolein ion is formed by losing three water molecules from the labile protonated molecular ion and represented as $[M+3-H_2O]$ [27]. The peaks detected at 691 m/z corresponds to the potassiated ion of diacylglycerol of CO. The presence of a diacylglycerol peak is attributed to the loss of one ricinoleic acid molecule as well as one/two water molecule from protonated diacylglycerol molecular ion $[M+2-H_2O]$ [27]. The less intense peak detected at 372.3 m/z represents the monoacylglycerol of CO [26]. The mass fraction of the components present in CO as obtained from MALDI TOF MS analysis are: triacylglycerol (72%) and diacylglycerol (12.5%).

The mass spectrum of MCO 0.2 for the range 200-1400 m/z is represented in Fig. 1(b), and it can be seen that the peak intensity at 956 m/z is lowered as compared to CO. The peaks at 676 m/z and 395 m/z representing diacylglycerol and monoacylglycerol, respectively, for pentaerythritol were more intense as compared to that of CO, confirming the transesterification of CO with pentaerythritol [26]. This also signifies the higher loss of ricinoleic acid moiety, which bears secondary OH group in CO and the forma-

tion of the molecular groups with higher content of the primary OH group. Additional peaks at 720 m/z (low intensity) and 411 m/z (high intensity) correspond to the sodiated diricinoleate and monoricinoleate of pentaerythritol [27]. This indicates that the transesterification of CO has led to the introduction of the primary OH group to CO since the monoricinoleate and diricinoleate represent three to two OH groups in terminal position. The medium intensity peaks at 395 and 337 m/z correspond to the pottasiated ions of mono-pentaeryhtritol ricinoleate-$2H_2O$ and pentaeryhtritol mono ricinoleate peaks of pentaerythritol [28]. The mass fraction of various components in MCO obtained from the MALDI MS analysis is as follows: diacylglycerol (20.5%), monoacylglycerol (39.9%), diricinoleate of pentaerythritol (8.5%) and monoricinoleate of pentaerythritol (19.5%). Thus, on the basis of these observations it can be claimed that the transesterification of CO using pentaerythritol was successful since the obtained MCO 0.2 contains monoricinoleates, diricinoletaes and monoacylglycerol com-
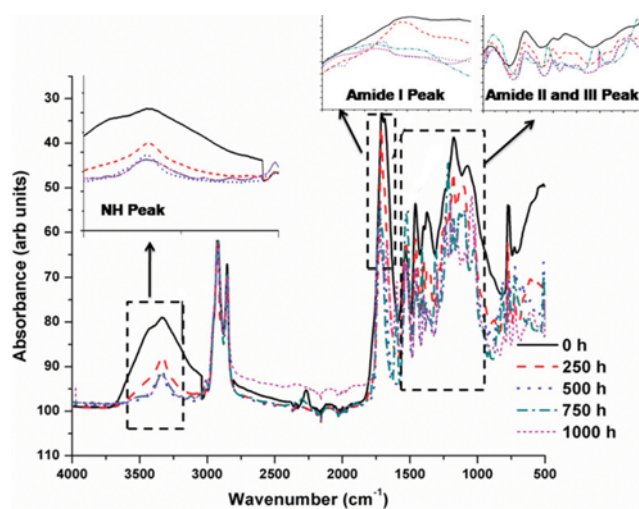

Fig. 2. FTIR representation of UBPU samples at (a) 0 h (b) 250 h (c) 500 h (d) 750 h (e) 1,000 h.
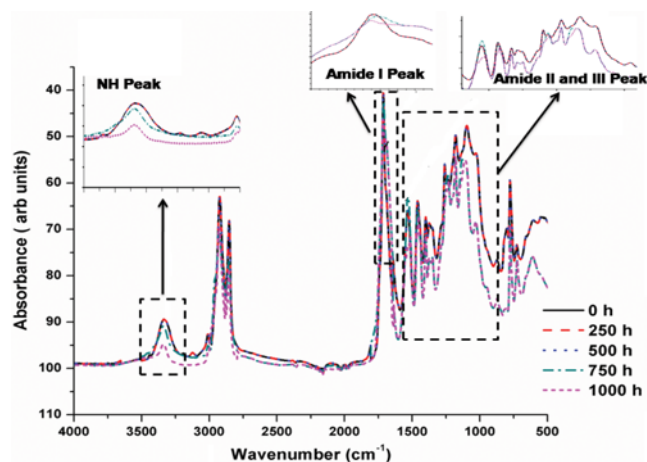
Fig. 3. FTIR representation of MBPU 0.2 samples at (a) 0 h (b) 250 h (c) 500 h (d) 750 h (e) 1,000 h.

ponents with higher intensity [26].

3. Structural Changes During UV Aging through FTIR Analysis

For analyzing the impact of transesterification on the UV resistance of polyurethanes, FTIR pattern of UBPU (polyurethane from castor oil and PoIs) and MBPU 0.2 (polyurethane from transesterified castor oil and PoIs) is summarized in Figs. 2 and 3. For a better insight regarding the chemical degradation mechanism, FTIR analysis was carried out after every 250 h of UV exposure. The FTIR spectrum of unexposed UBPU and MBPU 0.2 film showed characteristic absorption bands at 3,720-3,050 cm^{-1} (-NH stretching), 1,780-1,665 cm^{-1} (-C=O of urethane stretching vibration, Amide I), 1,531 cm^{-1} ($\upsilon_{C-C+C-N}$, Amide II) and 1260-1,252 cm^{-1} (υ_{C-N}, -NH bending, Amide III), respectively. The peak at 3,351 cm^{-1} in case of UBPU indicates the -NH group stretching vibration of non H-bonded urethane linkage, while the shift of the peak to 3,288 cm^{-1} in case of MBPU signifies -NH group vibration for H-bonded urethane linkage [NH....O=C] [29]. For UBPU the peak at 1,741 cm^{-1} represents the presence of non H-bonded free carbonyl group, while the presence of peak at 1,714 cm^{-1} indicates H-bonded carbonyl in disordered form [29]. On the other hand, the FTIR spectrum of MBPU 0.2 reveals a single peak at 1,713 cm^{-1} corresponding to the H-bonded carbonyl in disordered form. This shifting of -NH and C=O peak towards lower wavenumber might be due to the formation of H-bonds in different magnitude between the respective segments [30]. The formation of H-bonds in MBPU 0.2 depends upon the higher hydroxyl (OH) group and higher intermolecular interaction within the mutually attractive groups, i.e., OH of MCO and PoIs of NCO [31]. Being aliphatic and flexible with primary NCO group, PoIs can undergo higher reactivity towards the primary OH group in 1, 4 BD, resulting in higher H-bonded urethane linkages in MBPUs [32]. However, in case of UBPU the secondary OH group of CO, large amount of dangling chains and lower hydroxyl value create steric hindrance for the formation of complete H-bonded urethane linkages. Presence of peak at 2,260 cm^{-1} in case of UBPU indicates unreacted NCO group of PoIs; however, these bands were absent in case of MBPU 0.2, revealing a complete polymerization reaction.

However, a variation in FTIR peak and their intensities after

UV exposure of the samples was recorded. In case of UPBU, a drastic reduction in the peak area of the -NH band at 3,351 cm^{-1}, was observed, after 250 h, which decreased further with the increase in aging time. A steady decrease in the peak height corresponding to amide I, II and III peak nearly at 1,741 cm^{-1}, 1,531 cm^{-1} and 1,260 cm^{-1} respectively, was also observed after 250 h of UV exposure, revealing the chain scission of the urethane linkages. The reduction of C-C, C-O and C-H stretching vibration at 1,460 cm^{-1}, 1,238 cm^{-1} and 1,100 cm^{-1} respectively, suggests film erosion effect [1]. Additionally, a similar trend of decrease in the intensities was noticed at 2,926 cm^{-1} and 2,860 cm^{-1} peak that corresponds to CH$_2$ stretching, vibration. More interestingly, the peak corresponding to the unreacted NCO group at 2,260 cm^{-1} (noticed in unexposed UBPU) disappeared completely after UV exposure of 250 h, which might be due to the consumption of some remaining NCO group as a consequence of UV light. This particular observation corroborates the findings reported by Yang et al. [7]. However, for MBPU 0.2, the lowering of peak area and intensity corresponding to -NH vibration, amide bonds (i.e., I, II and III) and CH$_2$ stretching was initiated at around 750 h of UV exposure, which was higher than that of UBPU.

On the basis of the above observations, the possible mechanism of degradation of the PU systems used in this study is presented in Fig. 4. The substantial decrease in the intensity of the -NH band at 3,351-3,288 cm^{-1} signifies the loss of urethane structure due to the oxidation of -NH bonds under UV irradiation [9,34,35]. The UV irradiation provoked oxidation on the methylene group (-CH$_2$) in α position to the -NH group [36,37]. Subsequently, this oxidation reaction led to the formation of hydroperoxide (I), secondary peroxides (II), carbamic acid (III), disintegrated products (IV) and (V) [38,39]. The formation of this hydroperoxide compound led to the consumption of CH$_2$ group, resulting in a decrease in the intensity of absorption band at 2,926 cm^{-1} and 2,860 cm^{-1} respectively, for exposed UBPU and MBPU 0.2 films [37] as observed in Scheme 1. The hydroperoxide (I) group undergoes subsequent oxidation reaction in Scheme 2 resulting in the evolution of carboxylated products such as carboxylic acid (VI), aldehyde (VII), acetyl urethane (VIII), primary urethane (IX) and carbon dioxide gas (X) [33]. The reduction in peak height at 1,741-1,713 cm^{-1} corresponding to amide I band indicates decomposition of aliphatic ester structure (XI) on UV exposure as shown in Scheme 3 [1,9]. The steady decrease in the C-H, C-O and C-C stretching vibration can be attributed to the decomposition of instable carbamic acid (III) into an amine (XIV) and CO$_2$ gas (XV) (Scheme 4) [33,39]. The evaporation of CO$_2$ gas from the surface led to the decrease in the peak intensity of C-O, C-H and C-C groups [1,33].

Das et al. [40] reported that under UV aging the double bonds or allylic hydrogen present in the ricinoleic acid (XVI) of castor oil can undergo McLafferty type rearrangement reaction through a free radical mechanism to form heptalaldehyde (XVII) and undecylenic acid (XVIII) (Scheme 5). This imparts additional degradation reaction within the polyurethane system. From the MALDI-TOF analysis, it was confirmed that the amount of ricinoleic acid decreased after transesterification of castor oil, and that may cause the inhibited degradation of the MBPU 0.2 system as compared to that of UBPU. This is attributed to the relatively lesser ricinoleic
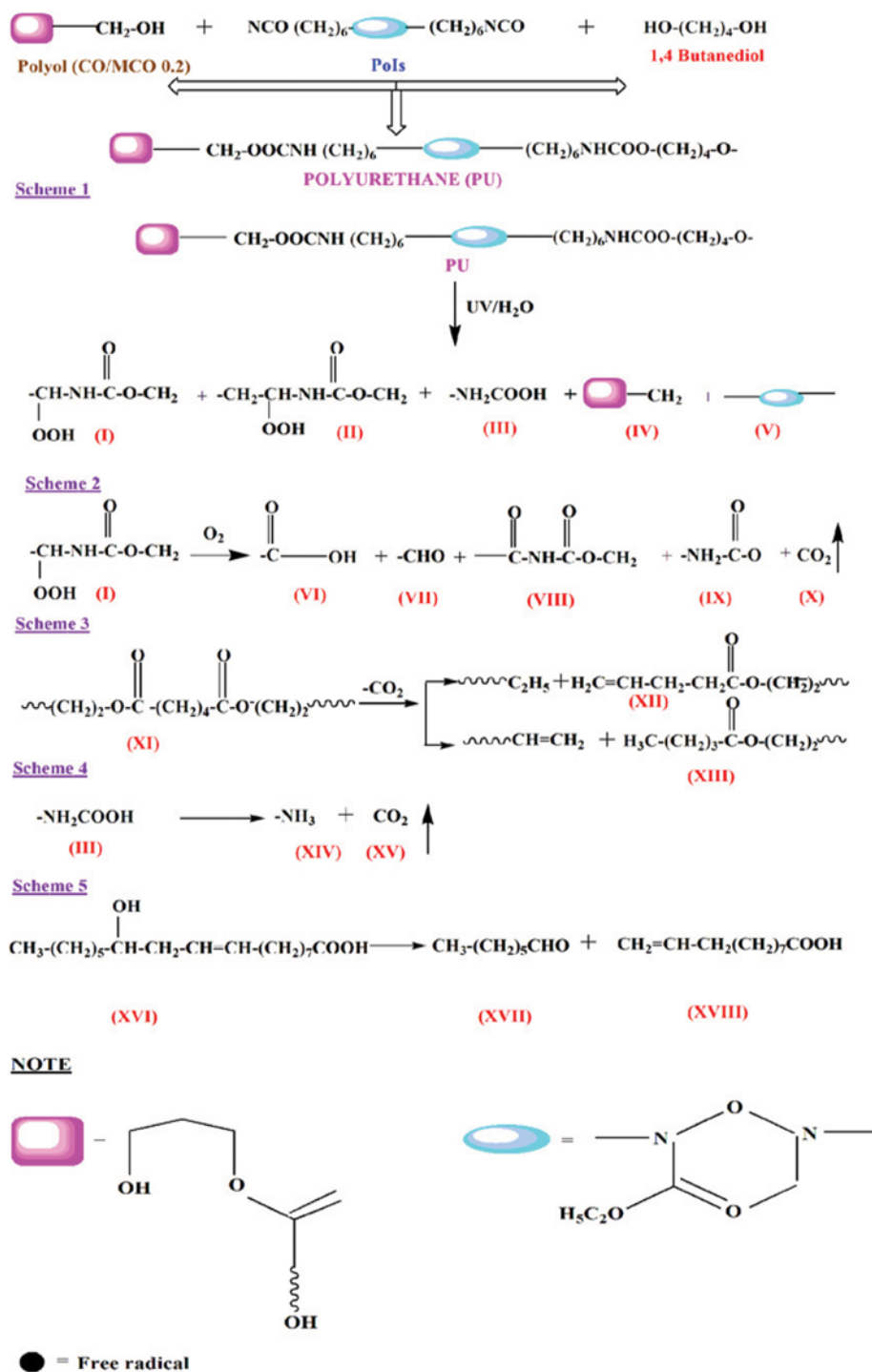
Fig. 4. UV aging mechanism of synthesized PU samples.

acid content in MBPU system, synthesized from transesterified castor oil.

The difference in initiation time towards degradation, 250 h for UBPU and 750 h, for MBPU 0.2 can be explained on the basis of the structural arrangement of the polymer. This observation can be correlated with the effective crosslinked network structure formed in MBPU 0.2 on account of higher OH number, increased urethane content and higher intermolecular interactions caused by H-bonding [32,41] thereby improving the anti-aging resistance characteristic against weathering. Therefore, a diminished chain scission effect was apparent in case of MBPU 0.2 which, although, occurred but started only after 750 h of UV exposure. While in case of UBPU the presence of relatively higher dangling series, longer fatty acid chain along with lower OH number in CO creates imperfections and plasticizing effect, which hinders the complete cross-linking reaction between the mutually attractive groups: OH of CO and
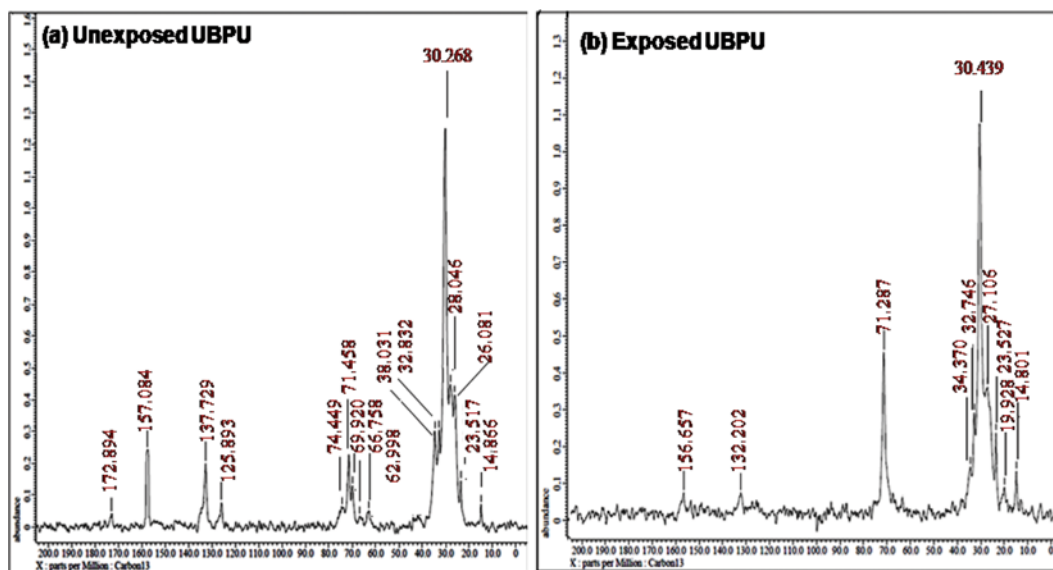
Fig. 5. ^{13}C NMR spectra of (a) Unexposed UBPU and (b) Exposed UBPU.
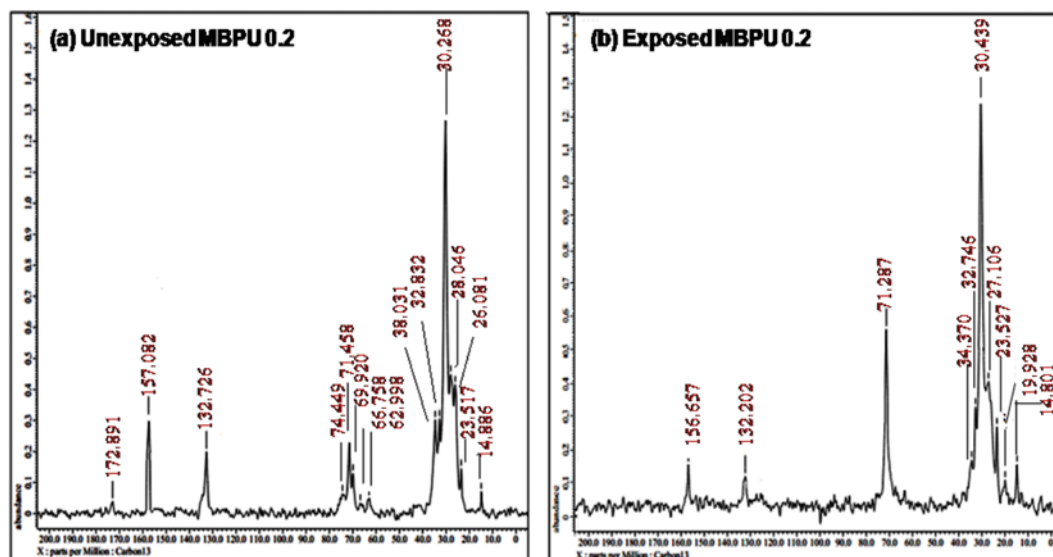

Fig. 6. ^{13}C NMR spectra of (a) Unexposed MBPU 0.2 and (b) Exposed MBPU 0.2.

NCO of PoIs. This results in the formation of defective network structure in UBPU, resulting in higher degradation under UV aging.

The FTIR results indicate that the photo-oxidative stability of PUs depends upon the intermolecular interactions, OH number of polyol and H-bonding. Hence, taking into account the above factors, it can be concluded that photo-oxidative stability of PUs in presence of transesterified CO based polyol with higher hydroxyl number is better as compared with PUs derived from raw CO with lower hydroxyl number. Further, the chemical interaction between POIs and 1, 4 BD can be advantageous for the development of UV-resistant bio-based coating materials.

4. Solid State Nuclear Magnetic Resonance Spectroscopy (NMR)

To better understand the degradation mechanism, solid state ^{13}C NMR studies were performed for PU samples before and after UV exposure. Fig. 5(a)-(b) represents the ^{13}C NMR spectra of un-

exposed and exposed UBPU, while Fig. 6(a)-(b) represents the ^{13}C NMR spectra of unexposed and exposed MBPU 0.2 film samples. The ^{13}C spectra of unexposed UBPU and MBPU 0.2 film samples showed the appearance of ester (-C=O) at δ=172.894 ppm, urethane (-C (O) ONH) peak at δ=157.084 ppm, unsaturated (C=C) linkage at δ=132.729 ppm, -OCH$_2$ linkage at δ=74.449 ppm, 71.458 ppm, -CH$_2$COO linkage at 62.920 ppm, (C (O) OCNH) at 66.758 ppm and 62.998 ppm, saturated (-CH$_2$) linkages- at δ=38.031-23.517 ppm and -CH$_3$ peak at 14.886 ppm [42,43]. The ^{13}C NMR spectrum of unexposed UBPU revealed a single peak at δ=125.893 ppm for unreacted NCO linkages, which is consistent with that reported earlier in the FTIR studies. On the other hand, no such peak was observed in the ^{13}C NMR spectrum of unexposed MBPU 0.2, indicating the complete conversion of NCO groups during the polymerization reaction as discussed earlier.

After UV exposure of 1,000 h the -NCO peak at δ=125.893 ppm completely disappeared in the exposed UBPU spectrum due to the similar reason as discussed in the FTIR section [7]. Also, the ester peak at 172.894 ppm totally vanished in case of exposed ones, which might be related to the disintegration of ester structure during UV exposure as observed in Fig. 4 [42]. Furthermore, the peak corresponding to urethane (-C (O)ONH) functional groups shifts to 156.657 ppm, with reduced intensity for both the exposed samples as compared to the unexposed ones. This confirms the loss of urethane structure in exposed PUs on account of oxidation of -NH bonds with the evolution of degradation products such as hydroperoxide [33,34]. Also, the peaks corresponding to the -OCH$_2$, -CH$_2$COO and (C (O) OCNH) linkage completely disappeared under UV exposure with the appearance of a single peak at 71.287 ppm for both the exposed PU samples. This single peak might be related to -CHO group, which is formed as an oxidation product during the UV degradation process as seen in Fig. 4. The intensity of saturated linkages at δ=38.031-23.517 ppm revealed noticeable decrease for both the exposed PU samples, which can be due to consumption of methylene linkages (-CH$_2$), during hydroperoxide formation as discussed in the earlier section. Thus, the above result was found to be in good agreement with the FTIR analysis and confirms the UV aging mechanism as discussed in the earlier section.

However, it can be observed from ^{13}C NMR spectra that the exposed MBPU 0.2 film sample is less prone to oxidation, since they exhibit lower reduction in the intensity of the aforementioned peaks. This can be explained on the basis of its higher crosslinking density and intermolecular interactions that improves its anti-
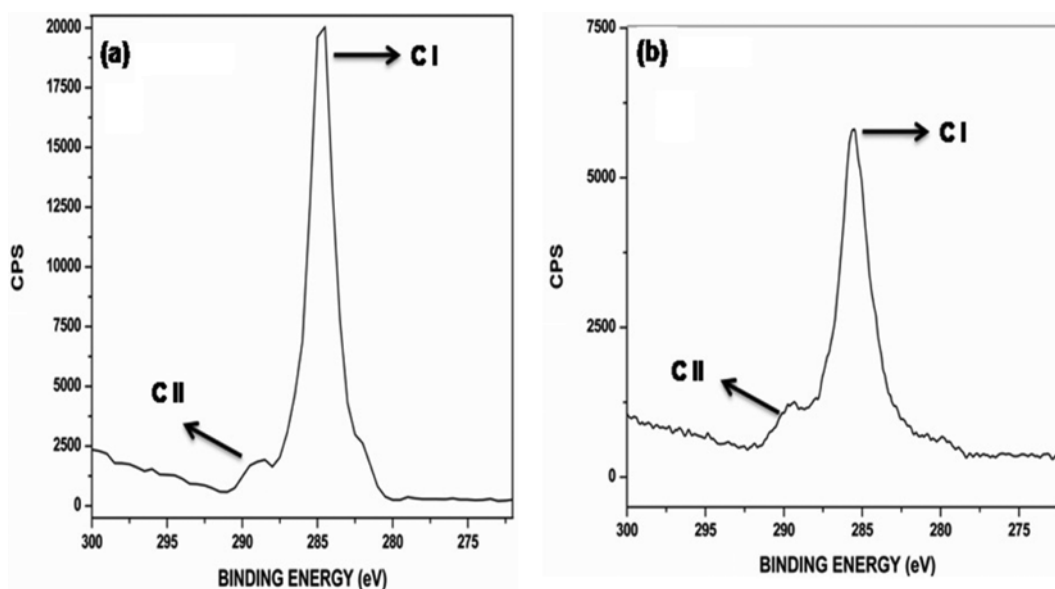

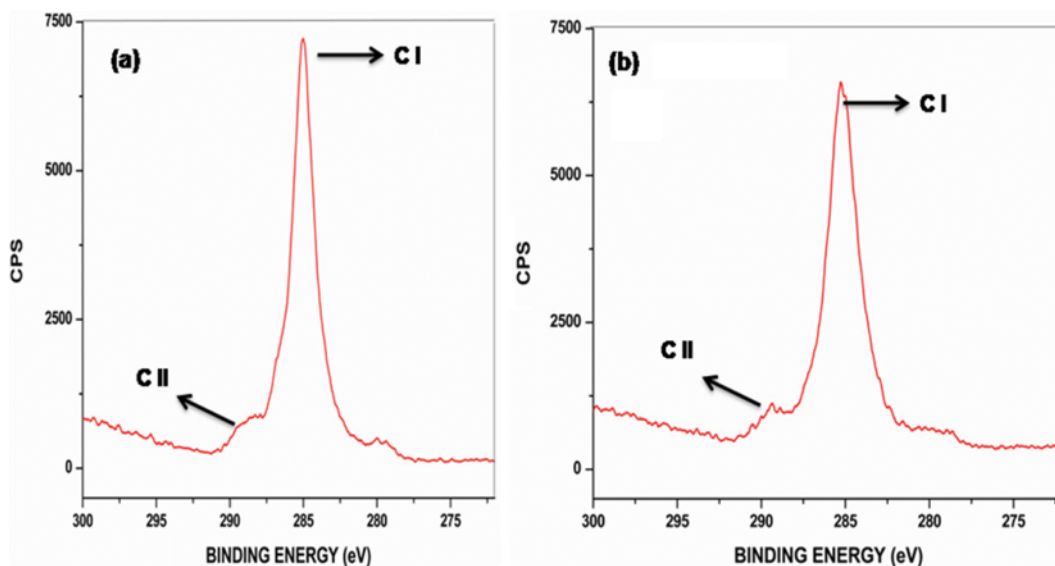Fig. 7. C1s spectra of (a) unexposed UBPU and (b) exposed UBPU.

Fig. 8. C1s spectra of (a) unexposed MBPU 0.2 and (b) exposed MBPU 0.2.

Table 4. Surface elemental composition of UBPU and MBPU 0.2 obtained from XPS analysis

Sample code	Atomic percentage (%)			Atomic ratio	
	C 1s	N 1s	O 1s	N1s/C1s	C1s/O1s
Unexposed UBPU (0 h)	945.2	57.9	541.8	0.06	1.74
Exposed UBPU (1,000 h)	929.9	77.8	621.9	0.08	1.49
Unexposed MBPU 0.2 (0 h)	1018.2	59.6	517.3	0.05	1.96
Exposed MBPU 0.2 (1,000 h)	1005.1	90.45	636.1	0.09	1.58

aging resistance characteristics. Hence, it is further proved that MBPU 0.2 can be used as UV-resistant coating with exceptional properties.

5. X-Ray Photoelectron Spectroscopy (XPS)

XPS analysis of the PU samples was performed before and after UV exposure for gaining better insight about the degradation mechanism of PU systems. Figs. 7 and 8 represent the C1s XPS spectra for UBPU and MBPU 0.2 before (0 h) and after (1,000 h) of UV exposure. Table 4 shows the changes in the surface elemental composition in terms of variation in carbon, oxygen and nitrogen content as well as the atomic ratios of carbon to oxygen (C1s/O1s) and nitrogen-to-carbon (N1s/C1s).

The C1s spectra of UBPU and MBPU 0.2 were characterized quantitatively before and after aging to assess the variation in the concentration of different functional groups, investigate the type of chemical bond and to identify the changes in chemical structure due to UV exposure [43,44]. It can be observed from Fig. 5(a) and 6(a) that before UV exposure (at 0 h) the C1s spectra of UBPU and MBPU 0.2 showed two prominent peaks. The first peak at 285 eV corresponds to C-H, C-C, C-N, C-O bonds and is assigned as C I. The second peak at 288.9 eV represents either N-C=O group obtained from urethane or carboxyl group (-COO) formed due to oxidation and is assigned as C II [45]. It was revealed from Fig. 5(b) and 6(b) that after UV exposure of 1,000 h the intensity of C 1s peaks at 285 eV and 288.9 eV decreases for both UBPU and MBPU 0.2. The reduction in the intensity of C 1s peak is due to the instability of carboxyl groups (-COO) which undergo chain scission resulting loss of oxidation products [45,46]. This corroborates well the degradation mechanism and FTIR results discussed earlier, confirming reduction of C-C, C-O and C-H groups after UV exposure.

Table 4 indicates that the nitrogen-to-carbon (N1s/C1s) ratio increases, while the carbon-to-oxygen (C1s/O 1s) ratio decreases after UV exposure for both UBPU and MBPU 0.2, respectively. For instance, the C 1s/O 1s ratio of UBPU after UV exposure decreases from 1.74 to 1.49, while for MBPU 0.2 it decreases from 1.96 to 1.58. The decrease in C 1s/O 1s ratio might be due to the loss of volatile oxidation products formed during the UV exposure [33]. On the other hand, the increase in the N1s/C1s ratio might be attributed to the formation of amide linkages after the oxidation of -NH bonds under UV irradiation. It is also observed from Table 4 that the atomic % decreases for carbon and increases for nitrogen as well as oxygen, respectively, after UV exposure for both the PU samples. This indicates that the surface of UBPU and MBPU 0.2 is oxidized after UV exposure as discussed in the FTIR studies. Furthermore, the UV irradiation causes scission of the long molecu-

lar chains present on the surface to form low molecular weight oxygen containing groups [43]. With increase in the irradiation time the number of chain scissions also increases, resulting in a significant increase in the atomic% of oxygen content. On the other hand, the decrease in the atomic% of carbon is due to the UV aging that initiates the chain scission and degradation of PU. The loss in carbon atomic wt% can also be attributed to the migration and volatility of oxidation products obtained from the degradation of carbonaceous products [44]. These results further correlate with the earlier discussion. Similar observations have been reported by Yuhan et al. and Wang et al. [43,44]. Thus, it is clear that UBPU and MBPU 0.2 films exhibit degradation due to UV exposure: however, the
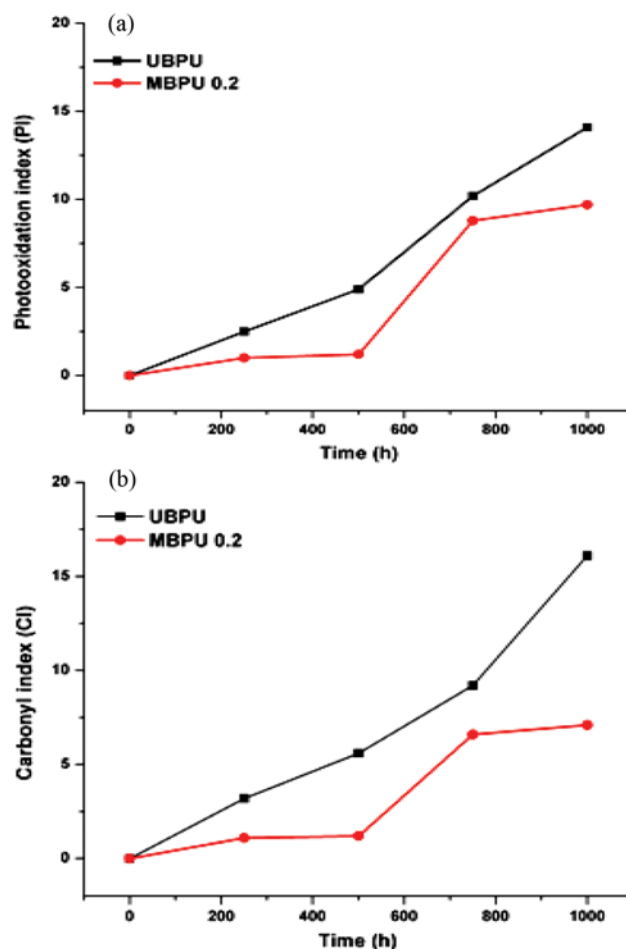

Fig. 9. (a) PI and (b) CI index of UBPU and MBPU 0.2 films as a function of UV exposure time.

latter indicated better UV aging resistance characteristics as compared to the former. This statement can be exemplified through the observed higher C 1s/O 1s ratio in case of exposed MBPU 0.2 film, which signifies its good anti-oxidation behavior against UV radiation [44]. The effective crosslinked network structure formed in MBPU 0.2 as explained in FTIR section resists the penetration of UV light, resulting in less damage to the molecular chain [44]. This further explains the observed less reduction in the intensity of C 1s peaks and atomic% of carbon respectively, in exposed MBPU 0.2 as compared to the corresponding UBPU ones.

6. Degradation Index (PI and CI)

The PI and CI indexes were evaluated to quantify the aging extent in UBPU and MBPU films, by taking into account the change in the intensity of peak area corresponding to υ (-NH) and υ (-C=O) band after UV exposure, keeping -CH peak as the internal standard. The higher the PI and CI index with respect to aging time higher is the degradation rate. It can be observed from Fig. 9 that both the PI and CI of UBPU increase linearly with increment in the UV exposure time, indicating chain scission. However, the change in CI and PI with increase in UV exposure time is much less in MBPU films as compared to UBPU film. For instance, at 250 h of UV aging, the PI of MBPU 0.2 is (1.075), which is much lower in comparison to that of UBPU film (1.13), respectively. Similar increasing trend with respect to UV exposure was noticed for CI values of MBPU 0.2 and UBPU. This confirms that the enhanced chemical interaction between the primary OH groups in MCO and aliphatic primary NCO groups in POIs along with higher hydroxyl number results in rigid and highly crosslinked structure,

which shields the passage of UV light, thereby prohibiting the degradation of MBPU films. Moreover, the higher number of H-bonds formed in MBPU can act as physical crosslinks, thereby increasing the intermolecular interaction, which can effectively suppress the rate of photo-oxidation reaction [32]. The above result corroborates the FTIR observations which revealed the presence H-bonded urethane carbonyl group peak in MBPU 0.2. Moreover, the OH number of the polyol has a linear relationship with the crosslinking density of the polyurethane [41]. Hence, the higher OH number of MCO 0.2 provides crosslinking site necessary for the formation of denser crosslinked network structure in the MBPU 0.2 film, resulting in suppression of photo-oxidative degradation rate. Further, the decrease in the intensity of peaks corresponding to the stretching vibration of -NH, urethane C=O observed in case of FTIR studies also validates the PI and CI results of UBPU and MBPUs, respectively.

Thus, it is suggested that the highly crosslinked structure of MBPU delays the rate of degradation process and the subsequent aging progression within it.

7. Morphological Analysis (SEM)

Figs. 10 and 11 show the SEM images of UV unexposed and exposed UBPU and MBPU 0.2 samples as a function of UV exposure. The unexposed film samples of UBPU and MBPU 0.2 at 0 h demonstrate a highly smooth surface with layered arrangement. However, after UV exposure morphological changes were observed due to photo-oxidative degradation, which is in line with the work reported earlier by Gulmine et al. and Cascaval et al. [47,48]. After UV exposure of 250 h blisters of diameter 250-300 nm were seen
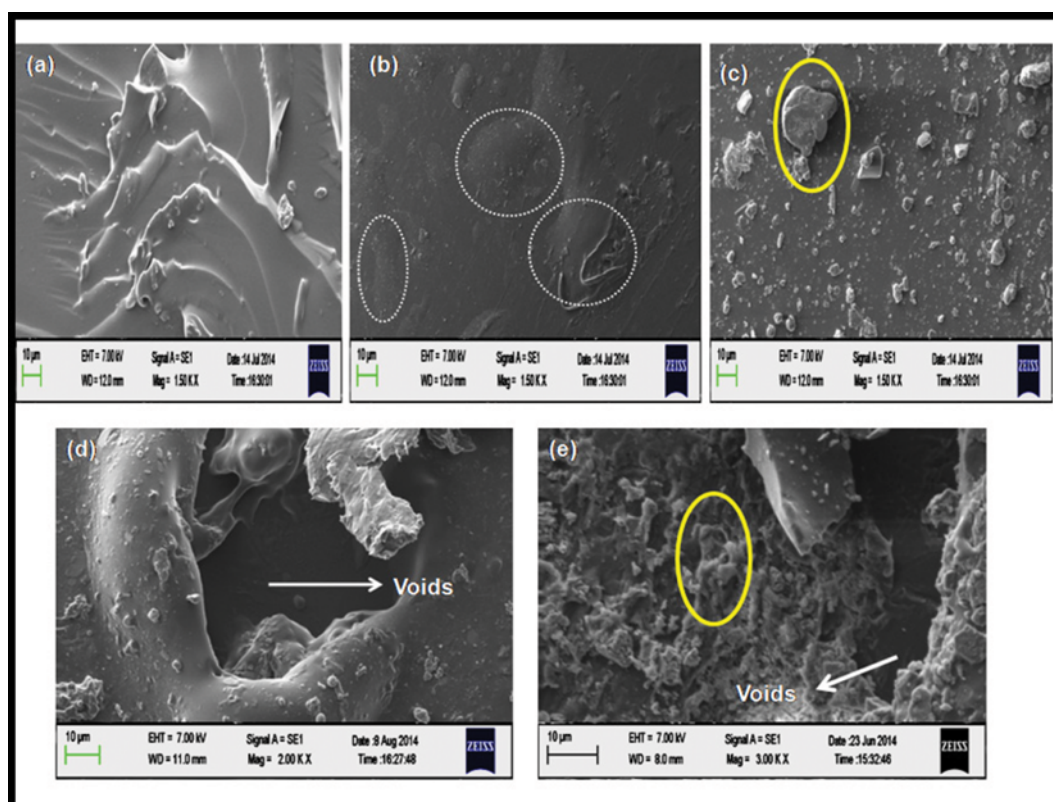

Fig. 10. Morphological changes in UBPU at (a) 0 h (b) 250 h (c) 500 h (d) 750 h and (e) 1,000 h.
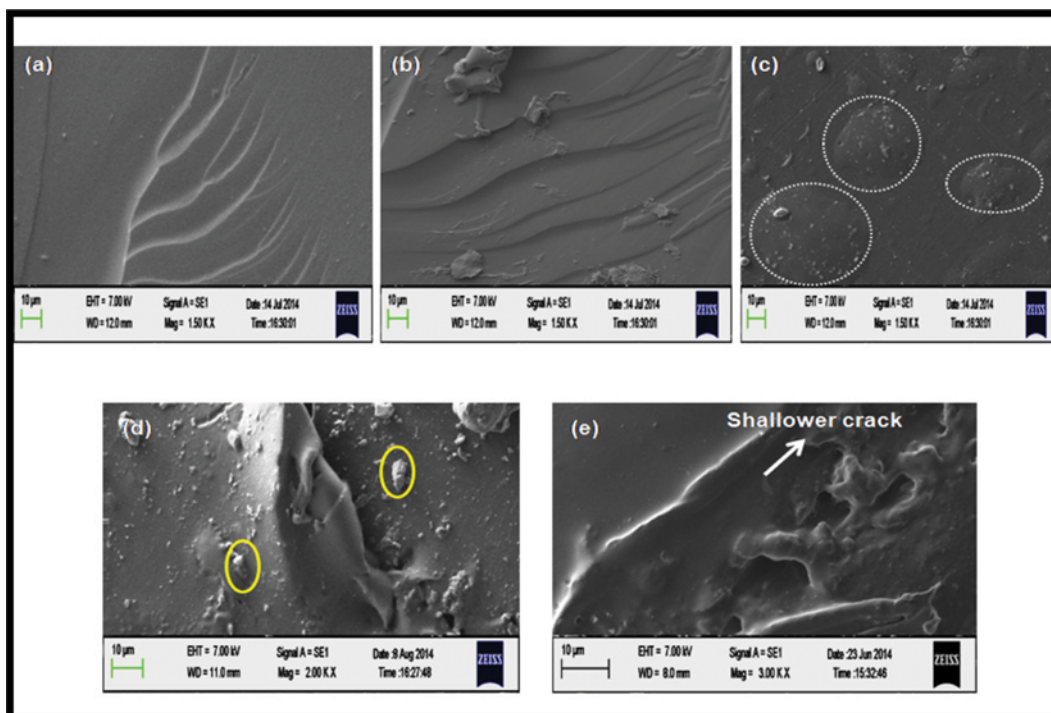
Fig. 11. Morphological changes in MBPU 0.2 at (a) 0 h (b) 250 h (c) 500 h (d) 750 h and (e) 1,000 h.

to protrude from the surface of exposed UBPU. The appearance of blisters is basically a physical mechanism which reveals the initial stage of the degradation process [7]. The possible reason behind blister formation is the alternating cycle of wet phase (i.e., condensation) and dry phase (i.e., UV) during the aging process [49]. During the dry phase the UV light provides radiation energy (hυ) to initiate the degradation process. During the condensation/wet phase, water, moisture and oxygen oxidize the PU surface, thereby forming oxidation products like hydroperoxide [49,50]. These oxidation products pierce through the PU surface, resulting in the formation of osmotic cells/blisters. An inhomogeneous osmotic pressure is created on the PU surface, and as a consequence the degradation products and water formed during the condensation phase cannot easily escape out during the dry phase. Owing to this osmotic pressure effect, blisters are formed on the PU surface under alternating UV and condensation process [7]. On the other hand, the noticeable blister formation began to form on the MBPU 0.2 surface only after 500 h of UV exposure with diameter ranging from 150-200 nm. The difference in exposure time required to initiate blister formation might be due to the stiffer and highly crosslinked network structure formed in case of MBPU 0.2 derived from MCO and POIs. As observed from FTIR the interurethane H-bonds formed in MBPU 0.2 act as physical crosslinks [51], which reinforces the amorphous phase and retards the degradation process. As a consequence, MBPU 0.2 surface provides a better barrier effect to the penetration of water, oxygen, free radicals and other side products like carbon dioxide, primary amine and hydroperoxide formed during the alternating UV and condensation process essential for accelerating photodegradation process. At the same duration of exposure, 500 h, the UBPU surface indicated the ap-

pearance of polymer fragments due to the breakage of blisters and loss of polymeric material, thereby damaging the surface layer. Later, after 750 h of UV exposure, holes and voids on the UBPU surface were observed, which might be due to molecular chain scission of urethane, carbon and ether bonds [44] generating polymer radicals under the influence of UV atmosphere and external stress like temperature and humidity. However, at the same time of exposure (i.e. 750 h) no noticeable crack propagation was observed in the MBPU film, while the appearance of polymer fragments was noticed due to the breakage of blisters as discussed above. Further, at 1,000 h of prolonged UV/condensation exposure it was revealed that there were deep voids with diameter ranging from 120-150 nm in UBPU surface. The formation of voids might be correlated with the excessive embrittlement caused due to the generation of radicals. These polymer fragments may give a branched chain structure of high molecular weight after getting attached to the main chain of the neighboring molecule, resulting in embrittlement and formation of cracks [10]. In addition, clustering of polymer fragments in the form of aggregates was observed covering the entire UBPU surface, which signifies higher rate of degradation due to huge loss of polymeric material. These aggregates are supposed to be the outcome of degradation products formed [7] as a consequence of exposure as indicated in the FTIR studies. On the other hand, for the same exposure time of 1,000 h the surface of MBPU 0.2 depicts no voids but rather shallower cracks with depth ranging from 40-50 nm This difference can be ascribed to the excellent barrier properties of stiffer polymer chains in MBPU 0.2 film that hinder the diffusion of species like free radicals and oxygen into the polymer surface to initiate the photo-degradation process. As a consequence, these species accumulate on the top surface,

Table 5. Glass transition temperature (T$_g$) of unexposed and exposed PU samples

UV exposure (h)	UBPU (T$_{gs}$) (°C)	UBPU (T$_{gh}$) (°C)	MBPU 0.2 (T$_{gs}$) (°C)	MBPU 0.2 (T$_{gh}$) (°C)
0	−25.1	59.7	−19.9	72.6
250	−34.8	46.7	−19.9	72.6
500	−42.5	44.8	−24.7	71.7
750	−44.4	41.8	−34	68.8
1000	−46.8	40.5	−39.6	56.2

causing degradation of the surface layer. Thus, shallower crack propagation occurs in MBPU 0.2 film surfaces as compared to UBPU. Further, there was less clustering of polymer fragments in the MBPU 0.2 surfaces.

Thus, these observations provide an insight that the highly cross-linked MBPU 0.2 film surface provides better photo-oxidation resistance to aging phenomenon for a long duration. Further, the above result corroborates the finding revealed in the FTIR section.

8. Differential Scanning Calorimetry (DSC)

The thermal analysis results (T$_g$) of the UV exposed UBPU and MBPU 0.2 samples are summarized in Table 5. The synthesized PUs exhibit two well defined glass transition temperatures, one corresponding to the soft segments (at negative temperature range, T$_{gs}$), and the other corresponding to the hard segment (at positive

temperature range, T$_{gh}$) [17,18]. There is a change in the T$_{gs}$ and T$_{gh}$ for both UBPU and MBPU 0.2 before and after UV exposure. This phenomenon might be due to the increase in flexibility and molecular mobility of the PU chain after UV exposure. As explained in the FTIR analysis, the oxidation reaction induced through UV light causes chain scission, which breaks the urethane linkage within the PU macromolecule. This breakage of the urethane linkage assists the facile movement of hard and soft segments within the polymer structure, and hence allows segmental mobility to form aggregates [34]. Thus, the UV exposed PUs show a remarkable decrease in T$_{gs}$ and T$_{gh}$ in comparison with the unexposed PU samples. Moreover, the decrease in tensile properties of the UV exposed PUs bears testimony to the increase in segmental mobility, while the formation of aggregates is well consistent with the SEM micrographs of the exposed PUs samples as discussed in the earlier sections. However, the drop in T$_{gs}$ and T$_{gh}$ values for exposed UBPU was comparatively higher than MBPU 0.2, which can be correlated with the higher crosslinked network structure formed in the latter, which effectively restricts the mobility of molecular chains even resulting in relatively difficult movement of hard and soft segments.

9. Tensile Tests

The effect of UV aging on the tensile properties of the PU films was analyzed and the results are summarized in Table 6. It is distinct that the tensile properties were relatively affected during the aging time for UBPU and MBPU 0.2 film.

Tensile modulus and tensile stress were found to be 18.6 MPa

Table 6. Effect of UV exposure on different properties of UBPU and MBPU 0.2

Characterization	Duration of UV exposure (h)				
	0	250	500	750	1000
(a) Tensile properties					
• Tensile stress $_{UBPU}$	14.2±0.1	10.1±0.3	9±0.4	8±0.4	5.5±0.1
• Tensile modulus $_{UBPU}$	18.6±0.4	14.1±0.1	12±0.5	10±0.2	6±0.3
• Tensile stress $_{MBPU\ 0.2}$	17.9±0.3	17.2±0.6	16.5±0.3	14±0.2	12±0.1
• Tensile modulus $_{MBPU\ 0.2}$	24.7±0.2	24±0.2	23.5±0.2	22.6±0.1	20.1±0.4
(b) Cross-linked fraction					
• CLF $_{UBPU}$ (wt%)	59±0.3	48±0.6	40±0.4	37±0.2	30±0.1
• CLF $_{MBPU\ 0.2}$ (wt%)	75±0.2	74.8±0.5	74.1±0.2	68±0.3	60±0.2
(c) Nanoindentation					
• E $_{UBPU}$ (GPa)	0.98±0.4	1.54±0.4	2.74±0.5	3.56±0.3	4.89±0.4
• E $_{MBPU\ 0.2}$ (GPa)	1.05±0.2	2.34±0.3	4.67±0.3	5.08±0.2	6.43±0.3
• H $_{UBPU}$ (GPa)	0.18±0.1	0.23±0.6	0.45±0.2	0.56±0.2	0.75±0.2
• H $_{MBPU\ 0.2}$ (GPa)	1.23±0.3	1.42±0.1	1.65±0.1	1.87±0.5	2.01±0.5
(d) Wettability analysis					
• Θ_{UBPU}	83.5±0.4	78.9±0.3	70.3±0.5	65.4±0.4	65±0.5
• $\Theta_{MBPU\ 0.2}$	89.9±0.1	89±0.3	88.2±0.5	87±0.5	86.8±0.2
• SFE$_{UBPU}$	65±0.3	63.4±0.2	62±0.1	60.1±0.4	58.3±0.4
• SFE$_{MBPU\ 0.2}$	70.1±0.4	69.4±0.6	68.3±0.3	62.1±0.1	60.1±0.5
(e) Aesthetic analysis					
• ΔE*$_{UBPU}$	0	3.8±0.3	4.6±0.4	6±0.3	6.4±0.1
• ΔE*$_{MBPU\ 0.2}$	0	3±0.4	3.4±0.5	4.1±0.2	5.8±0.2
• DYI $_{UBPU}$	0	4±0.1	4.6±0.1	5.3±0.4	6.9±0.2
• ΔYI $_{MBPU\ 0.2}$	0	2.1±0.3	2.9±0.3	3.2±0.3	3.9±0.1

and 14.2 MPa and 10.1 MPa, and for MBPU 0.2 it was 24.7 MPa and 17.9 MPa, respectively. After UV exposure of 250 h, tensile modulus and tensile stress of UBPU were found to decrease to the tune of 24% and 28.8%; however, no noticeable reduction was observed in the case of MBPU 0.2. Moreover, a reduction in tensile stress and modulus of UBPU and MBPU 0.2 was noticed with an increase in the exposure time, wherein MBPU 0.2 exhibited relatively less reduction in the mechanical properties. With the increase in the duration of UV exposure to 1,000 h, UBPU exhibited a decrease of 67% and 61.2% in the tensile stress and modulus, whereas a small reduction of 18.6% and 32.9% was noticed in the tensile stress and modulus of MBPU 0.2.

This lowering in the tensile properties is attributed to the light-induced chemical degradation, which includes chain scission and oxidation of the polymer [52], which is in accordance with the FTIR results. The chain scission phenomenon breaks the polymer chain and reduces the intermolecular interaction. This leads to easy penetration of water molecules [53] during the wet phase, which increases the molecular chain flexibility. As a result, the secondary links liable for material cohesion get destroyed, thereby weakening the internal structure. In fact, this plasticization effect can also lead to the rupture of secondary links (H-bonding interactions) within the polymer chains, leading to an increase in molecular mobility [54,55]. Thus, the above factors are conducive for increasing the free volume and decreasing the tensile strength, modulus with increment in duration of UV exposure.

The less reduction in the tensile properties of MBPU 0.2 can be attributed to the shorter chain length between the crosslink points of MBPU 0.2, which overshadows the relative rate of chain scission effect in comparison to the UBPU film sample. Also, the interlocked network structure formed in MBPUs owing to a greater association of MCO and POIs accounts for the higher crosslinking density and stronger interactions within the segments, resulting in the formation of effective barrier to the external destroying forces. Therefore, it may be concluded that transesterification of castor oil imparts enhanced UV resistance to the polyurethane. Further, the results obtained are in agreement with that observed in DSC studies as discussed in earlier section.

10. Cross-linked Fraction (CLF)

To further validate the impact of UV aging on the observed tensile and thermal behavior of exposed PU samples, the cross-linked fraction was calculated through sol-gel study and the findings are depicted in Table 6. The sol gel analysis of the unexposed MBPU 0.2 films indicates a CLF value of 75%, while the unexposed UBPU film reveals a CLF value of 59%. At 1,000 h of UV aging the CLF of UBPU and MBPU 0.2 was found to decrease to 30% and 60%, respectively, indicating breakage of long macromolecular chain into short chain. This may be due to photodegradation effect, which accelerates the chain scission and oxidation of PU bonds, resulting in diminished cross-linking density and loss of network integrity under exposure. However, it is clear from Table 5 that the loss in CLF wt% for exposed MBPU 0.2 films was less as compared with the exposed UBPU films, which supports the rigid network structure formed in the former and hence its UV resistant behavior. The decrease in CLF values after exposure to UV radiation validates the observed lowering of tensile properties and glass transition

temperature (T_g) for both MBPU 0.2 and UBPU film.

11. Nanoindentation

Table 6 shows the hardness (H) and elastic modulus (E) values of unexposed and exposed PU samples with respect to the duration of UV exposure. With UV irradiation the hardness (H) and elastic modulus (E) values of both the PU samples increase with subsequent increment in the exposure time. However, the unexposed MBPU sample exhibits higher hardness and elastic modulus value as compared with the corresponding unexposed UBPU sample. This observation can be correlated with the higher OH value of MCO, which favors higher cross-linking density and stiffness in MBPU 0.2, thereby increasing the resistance against penetration of indenter [55,56]. The UBPU film based on the lower OH value of CO has a higher plasticity index, which facilitates more plastic deformation as compared to elastic deformation, leading to lower hardness and elastic modulus value [55,56]. The results obtained are in agreement with that reported previously by Azvedo et al. and Yahyaei et al. [8,57].

Eventually, for the exposed UBPU and MBPU film the reduction in crosslinking density should lead to lower values of elastic modulus and hardness, respectively, but the reverse phenomenon is observed in case of nanoindentation. UV irradiation promotes a significant increase in the elastic modulus and hardness value for both the exposed UBPU and MBPU film, respectively, with an increase in exposure time, which can be ascribed to the formation of higher number of chemical bonds at the surface on account of the oxidation reaction [8] that resist the penetration of the indenter. The increase in elastic modulus for the exposed UBPU and MBPU films can be attributed to the physical aging mechanism that occurs in polymers subjected to UV weathering [58]. Physical aging increases the stiffness of the polymer both at the surface and the bulk as well as reduces the number of elastically inactive chains, i.e., dangling chains in the exposed polymer samples [59,60]. The preferential reduction of the dangling chains decreases the molecular mobility and promotes relaxation of the polymer network into a conformation that can accommodate the loss in material, resulting, in an increase in the elastic modulus of the exposed PU samples [60].

12. Wettability Analysis

Table 6 shows the calculated contact angle and surface free energy values of PU films before and after UV exposure. The unexposed MBPU 0.2 film exhibits higher contact angle as compared to the unexposed UBPU film due to higher crosslinking density in the former, which decreases the absorption of probe liquids within its surface [61]. However, with exposure the contact angle value decreases for both the exposed PU samples being more prominent in UBPU. The lowering of contact angle is due to the influence of UV irradiation, which is linearly proportional to the exposure time, resulting in alteration of the surface chemistry through the appearance of cracks and holes as observed in SEM studies [62]. These cracks and holes on the surface of exposed PU films promote absorption of probe liquids, resulting in higher wettability and lower contact angle. Additionally, the lowering of surface energy values (SFEs) in the exposed PU samples provides evidence that certain chemical changes might have occurred on the film surface due to degradation of polyurethane polymers during UV
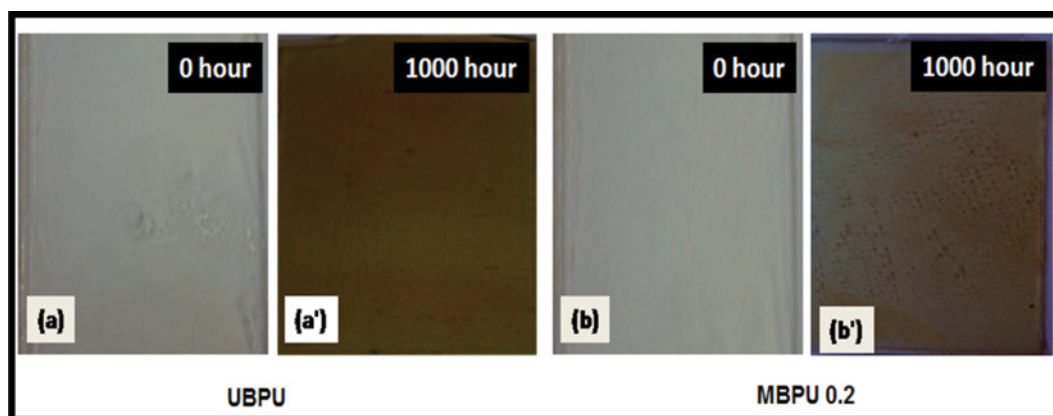
Fig. 12. Color change of unexposed and exposed UBPU and MBPU 0.2 film samples.

exposure [63,64]. Hence, the surface becomes more hydrophilic after UV exposure.

13. Aesthetic Analysis (Color Difference and Yellowness Index)

To access the impact of UV exposure on the aesthetic behavior, the color difference (ΔE^*) and the yellowness index (ΔYI) of UBPU and MBPU 0.2 film as a function of exposure time were investigated. Lower the value of ΔE^* and ΔYI, the higher is the resistance of the film against discoloration and vice versa. It is evident from Table 6 and Fig. 12 that there is change in color for both the PU samples after UV exposure from being colorless to yellow. This color change is attributed to the oxidation reaction leading to the loss of urethane structure [9]. A satisfactory agreement between the calculated ΔE^* and FTIR observation was found in both the exposed PU samples. An appreciable change in ΔE^* value was observed for UBPU samples at 250 h of UV exposure, which increased with increase in UV exposure time. While for MBPU 0.2 samples the change in ΔE^* value was prominent after 750 h of UV exposure. This indicates that MBPU 0.2 showed less deterioration towards UV exposure as compared to UBPU, which may be attributed to the highly interconnected molecular structure formed in the former during polymerization reaction. Due to the rigid network structure and higher urethane content in MBPU 0.2 the rate of photo-oxidation is reduced, resulting in improved resistance against discoloration. However, in UBPU the lower crosslinking as discussed above and weaker interactions within castor oil and POIs enhance the rate of photo-oxidative degradation, leading to more oxidation and subsequent yellowing of films. Similar trend of linear increase in ΔYI was observed for both the PU films. However, the lower ΔYI observed for MBPU 0.2 as compared to UBPU indicates higher crosslinking in the former, which improves the light resistance of the material by delaying the aging process. For convenience, we have represented the images of both the PU samples before UV exposure, 0 h and after 1,000 h of UV exposure, in Fig. 8 to show the color change.

Thus, the markedly lower values of ΔE^* and ΔYI for MBPU 0.2 confirm its enhanced photo-oxidative stability.

CONCLUSION

Green polyurethane was successfully synthesized using biobased castor oil and transesterified castor oil with palm oil based isocyanate (PoIs) in presence of 1, 4 butanediol as chain extender. The respective green polyurethanes were investigated to assess the UV aging characteristics at different exposure times of 0 h, 250 h, 500 h, 750 h and 1,000 h, respectively. On the basis of physicomechanical properties, MBPU 0.2 was considered to be the optimum composition with balanced solvent consumption and viscosity essential for easy coating applicability. The FTIR results provide evidence regarding the UV degradation of the exposed polyurethane samples through lowering of υ (-NH), υ (C=O) and υ (-CH$_2$) stretching vibration peaks. However, MBPU 0.2 films indicated lowering of peak intensities after 750 h of prolonged exposure, which was higher as compared to UBPU. XPS and ^{13}C NMR studies also suggested noticeable changes in the chemical linkages of the polyurethane films subjected to UV irradiation. SEM micrographs revealed the appearance of blister and crack on the exposed film surface due to chalking out of the polyurethane binder. However, MBPU 0.2 indicated shallower crack propagation which might be due to higher hydroxyl value of the precursor transesterified castor oil (i.e., MCO 0.2) that led to the formation of highly crosslinked structure.

Thus, castor oil can be effectively modified by transesterification reaction to synthesize green polyurethane coatings and films with improved UV aging resistance characteristics. Future studies will focus on the development of durable UV resistant green polyurethane coatings from transesterified castor oil and palm oil based isocyanate. In addition, a comparative analysis will be carried out between the developed durable UV resistant green polyurethane coatings with the commercial ones in our next study.

ACKNOWLEDGEMENT

REFERENCES

1. S. Bhargava, M. Kubota, R. D. Lewis, S. G. Advani, A. Prasad and J. M. Deitzel, *POC*, **79**, 75 (2015).
2. P. K.Maji, P. K. Gucchait and A. K. Bhowmick, *J. Mater. Sci.*, **21**,

5861 (2009).

3. A. Wolska, M. Goździkiewicz and J. Ryszkowska, *J. Mater. Sci.*, **47**, 5627 (2012).

4. J. Zhang, W. Tu and Z. Dai, *POC*, **75**, 579 (2012).

5. F. L. Floyd, *Risk Management: The Real Reason for Long Product Development Time Cycles*, ACS Symposium Series (1999).

6. J. W. Martin, *Service life prediction of polymeric material: Global perspectives*, Springer Science and Business Media, New York (2009).

7. X. F. Yang, D. E. Tallman, G. P. Bierwagen, S. G. Croll and S. Rohlik, *Polym. Degrad. Stab.*, **77**, 103 (2002).

8. E. C. Azevedo, E. M. Nascimento, G. O. Chierice, S. C. Neto and C. M. Lepienski, *Polímeros.*, **23**, 305 (2013).

9. D. Rosu, L. Rosu and C. N. Cascaval, *Polym. Degrad. Stab.*, **94**, 591 (2009).

10. A. Boubakri, N. Guermazi, K. Elleuch and H. F. Ayedi, *Mater. Sci. Eng. A.*, **527**, 1649 (2010).

11. Y. Zhang, J. Mexted, A. Barber, C. Lowe and R. Smith, *Polym. Degrad. Stab.*, **98**, 527 (2013).

12. V. Garcia-Pacios, V. Costa, M. Colera and J. M. Martin-Martinez, *POC*, **71**, 136 (2011).

13. M. F Valero and A. Gonzalez, *J. Elastomers Plast.*, **44**, 433 (2012).

14. M. Szycher, *Szycher's Handbook of Polyurethanes*, 2nd Ed., CRC Press (2012).

15. M. Ionescu, *Chemistry and Technology of Polyols for Polyurethanes*, Smithers Rapra Publishing (2005).

16. P. S. Suchithra, V. K. Abitha, D. Patil and A. V. Rane, *Mor. J. Chem.*, **3**, 476 (2015).

17. S. Das, P. Pandey, S. Mohanty and S. K. Nayak, *Mater. Express.*, **5**, 377 (2015).

18. S. Das, P. Pandey, S. Mohanty and S. K. Nayak, *POC*, DOI:10.1016/j.porgcoat.2016.04.012.

19. H. Wang, Y. Wang, D. Liu, Z. Sun and H. Wang, *J. Nanomaterials* (2014), DOI:10.1155/2014/487343.

20. Y. S. Lai, C. W. Tsai, H. W. Yang, G. P. Wang and K. H. Wu, *Mater. Chem. Phys.*, **117**, 91 (2009).

21. W. Wu and G. Nancollas, *Adv. Colloid Interface Sci.*, **79**, 229 (1999).

22. D. K. Owens and R. C. Wendt, *J. Appl. Polym. Sci.*, **13**, 1741 (1969).

23. Indian Standard Specification: Methods of Sampling and Test for Resins for Paints: IS 354 (1981).

24. G. S. Wooster, Hamburg and F. M. Delgado, US Patent 3,639,355 (1972).

25. K. Somani, S. Kansara, R. Parmar and N. Patel, *Int. J. Polym. Mater.*, **53**, 282 (2004).

26. M. Valero, J. Pulido, A. Ramirez and Z. Zhendong, *J. Am. Oil Chem. Soc.*, **86**, 383 (2009).

27. A. Kaushik and P. Singh, *Int. J. Polym. Anal. Charact.*, **10**, 373 (2005).

28. M. F. Valero, J. E. Pulido, A. Ramirez and Z. Cheng, *Qimica Nova.*, **31**, 2076 (2008).

29. T. Gurunathanan, S. Mohanty and S. K. Nayak, *POC*, **80**, 39 (2015).

30. M. A. de Luca, M. Martinelli, M. M. Jacobi, P. L. Becker and M. F. Ferrao, *J. Am. Oil Chem. Soc.*, **83**, 147 (2006).

31. M. M. Coleman, K. H. Lee, D. J. Skrovanek and P. C. Painter, *Macromolecules*, **19**, 2149 (1986).

32. G. Lligadas, J. C. Ronda, M. Galia and V. Cadiz, *Biomacromolecule.*, **8**, 686 (2007).

33. X. F. Yang, C. Vang, D. E. Tallman, G. P. Bierwagen, S. G. Croll and

S. Rohlik, *Polym. Degrad. Stab.*, **74**, 341 (2001).

34. R. N. Jana and H. Bhunia, *High Performance Polym.*, **22**, 3 (2010).

35. V. Romanova, V. Begishev, V. Karmanov A. Kondyurin and M. F. Maitz, *J. Raman Spectrosc.*, **33**, 769 (2002).

36. C. Willhelm and J. L. Gardette, *Polym.*, **39**, 5973 (1998).

37. B. Claude, L. Gonon, V. Verney and J. L. Gardette, *Polym. Test.*, **20**, 771 (2011).

38. L. Irusta and M. J. Fernandez-Berridi, *Polym. Degrad. Stab.*, **63**, 113 (1999).

39. H. Kim and M. W. Urban, *Langmuir*, **16**, 5382 (2000).

40. G. Das, R. K. Trivedi and A. K. Vasishtha, *JAOCS*, **66**, 938 (1989).

41. A. Zlatanic, C. Lava, W. Zhang and Z. S. Petrovic, *J. Polym. Sci., Part B: Polym. Phys.*, **42**, 809 (2004).

42. D. J. Harris, R. A. Assink and M. Celina, *Macromolecules*, **34**, 6695 (2001).

43. C. S. Wong and K. H. Badri, *Mater. Sci. Appl.*, **3**, 78 (2012).

44. L. Yuhan, L. Yuxi, L. Shazou and T. Huifeng, *J. Wuhan University of Technology-Mater. Sci. Ed.*, **29**, 1270 (2014).

45. Z. Y. Wang, F. C. Liu, E. H. Han, K. E. Wie and L. SuZhen, *Chinese Sci. Bull.*, **54**, 3464 (2009).

46. Y. Deslandes, G. Pleizier and D. Alexander, *Polym.*, **39**, 2361 (1998).

47. J. V. Gulmine and L. Akcelrud, *Eur. Polym. J.*, **42**, 553 (2006).

48. C. N. Cascaval, C. Ciobanu, D. Rosu and L. Rosu, *J. Appl. Polym. Sci.*, **83**, 138 (2002).

49. X. F. Yang, J. Lib, S. G. Croll, D. E. Tallman and G. P. Bierwagen, *Polym. Degrad. Stab.*, **80**, 51 (2003).

50. J. Lemaire, R. Arnaud and J. Gardette, *Pure Appl. Chem.*, **55**, 1603 (1983).

51. Z. W. Wicks, F. N. Jones and S. P. Pappas, *Organic coatings science and technology*, 2nd Ed., Wiley New Jersey (1994).

52. C. Prisacariu, *Polyurethane Elastomers: From Morphology to Mechanical Aspects*, Springer Science & Business Media, New York (2011).

53. A. Tidjani, *J. Appl. Polym. Sci.*, **64**, 2497 (1997).

54. A. Boubakri, N. Haddar, K. Elleuch and Y. Bienvenu, *Mater. Des.*, **31**, 4194 (2010).

55. M. P. Foulc, A. Bergeret, L. Ferry, P. Ienny and A. Crespy, *Polym. Degrad. Stab.*, **89**, 461 (2005).

56. H. Ghermezcheshme, M. Mohseni and H. Yahyaei, *Tribol. Int.*, **88**, 66 (2015).

57. H. Yahyaei and M. Mohseni, *Tribol. Int.*, **57**, 147 (2013).

58. G. Wypych, *Handbook of material weathering*, ChemTec Publishing, Toronto (1995).

59. A. W. Signor, M. R. VanLandingham and J. W. Chin, *Polym. Degrad. Stab.*, **79**, 359 (2003).

60. A. Skaja, D. Fernando and S. Croll, *JCT Res.*, **3**, 41 (2006).

61. H. H. Wanga, J. Mou, Y. H. Ni, G. Q. Fei, C. L. Si and J. Zou, *Express. Polym. Lett.*, **7**, 443 (2013).

62. P. Kuang and K. Constant, *Increased Wettability and Surface Free Energy of Polyurethane by Ultraviolet Ozone Treatment*, In Tech Publishing, US (2015).

63. N. Nuraje, S. I. Khan, H. Misak and R. Asmatulu, *ISRN Polym. Sci.*, **8** (2013), DOI:10.1155/2013/514617.

64. A. Mohammad Rabea, M. Mohseni, S. M. Mirabedini and M. Hashemi Tabatabaei, *Appl. Surf. Sci.*, **258**, 4391 (2012).